FINITE ELEMENT ANALYSIS OF THE TEMPERATURE DISTRIBUTION IN FRICTION STIR WELDING

Mauricio Rangel Pacheco, pacheco@esss.com.br
ESSS – Avenida Presidente Vargas, 3131 - 12º andar – 1203 – Centro Empresarial Cidade Nova - 20210-031
Rio de Janeiro – RJ - Brazil
CEFET/RJ - PPEMM - Programa de Pós-Graduação em Engenharia Mecânica e Tecnologia de Materiais
Av. Maracanã, 229, 20271-110 - Rio de Janeiro - RJ – Brasil

Pedro Manuel Calas Lopes Pacheco, calas@cefet-rj.br
CEFET/RJ - PPEMM - Programa de Pós-Graduação em Engenharia Mecânica e Tecnologia de Materiais
Av. Maracanã, 229, 20271-110 - Rio de Janeiro - RJ – Brasil

Abstract. *Welding is a fabrication process widely used in several industrial areas. The welding of metallic alloys presents some basic characteristics as the presence of a localized intensive heat input that promotes mechanical and metallurgical changes. Temperature gradients developed through the piece promotes residual stresses fields when the piece reaches room temperature. Phenomenological aspects of welding involve basically three couplings: thermal, phase transformation and mechanical phenomena. Different from conventional welding processes, where macroscopic fusion is observed, friction welding is a solid state welding process where the joint is produced by the relative rotational and/or translational motion of two pieces under the action of compressive forces producing heat and plastic strain on the friction surfaces. Friction Stir Welding (FSW) process has received much attention for its special characteristics, like the high quality of the joints. Although there are several experimental works on the subject, numerical modeling is not well stated, as the process is very complex involving the coupling of several non-linear phenomena. In this contribution tridimensional and bidimensional finite element models are presented to study the temperature distribution in plates welded by the FSW process. A weld heat source is proposed to represent the heat generated during the process. The heat source model considers several contributions present in the process as the friction between the tool and the piece and the plastic power associated to the plastic strain developed. Numerical results show that the models are in close agreement with experimental results, indicating that the models are capable of capturing the main characteristics of the process. The proposed models can be used to predict important process characteristics, like the TAZ (Thermal Affected Zone), as a function of the welding parameters.*

Keywords*: Friction Stir Welding, Modeling, Finite Element Method*

1. INTRODUCTION

Welding is a fabrication process widely used in several industrial areas. The welding of metallic alloys presents some basic characteristics as the presence of a localized intensive heat input that promotes mechanical and metallurgical changes. The temperature gradients developed through the piece promotes residual stresses fields when the piece reaches room temperature. Phenomenological aspects of welding involve basically three couplings: thermal, phase transformation and mechanical phenomena. Welding process can be classified by the type of the heat source used and can involve metal fusion or not. Conventional welding processes, like TIG and laser, involve the metal fusion promoted by a highly localized heat source. Near the welding joint a Heat Affected Zone (HAZ) develops, where microstrutural alterations and residual stresses are present. Friction welding process is a solid state process where metal fusion does not occur. Friction Stir Welding (FSW) is a welding process that has received much attention for his special characteristics, like the high quality of the joints. In this process the heat is generated by an intense mechanical work due friction between the pieces to be welded and a welding tool with rotational and transverse movements. The welded material softens at a temperature lower than the melting point, generating a weld joint with lower levels of residual stress and distortion than conventional fusion welding processes (Chen and Kovacevic, 2003). Figure 1 shows a schematic representation of the FSW process.

In FSW process three zones develop (Russell, 2000): Heat Affected Zone (HAZ), Thermomechanically Affected Zone (TMAZ) and Weld Nugget Zone (WNZ). The WNZ experiments extensive plastic strain and softening, and usually results in a fine equiaxed grain recristallized structure. The TMAZ experiments a lower level of plastic strain and is a relative small region surrounding the WNZ with a distorted grain structure. Finally the HAZ is the weakest region in the FSW. Figure 2 presents a schematic view of the three regions.

Although there are a considerable number of references in experimental works related to FSW process, relatively, a reduced number references on modeling and numerical simulation of the process are available. Modeling the FSW process results in a complex problem involving the coupling of mechanical and thermal non-linear phenomena. Several authors have addressed these aspects separately: from uncoupled hybrids approaches considering combined experimental data and numeric results, to models considering the coupling of the several phenomena (Colegrove *et al.*,

2000; Den and Xu, 2001; Chen and Kovacevic, 2003; Nadan *et al.*, 2006, 2008). Some authors present analytic models based on Rosenthal (1946) classic solution for a moving point heat source with a constant speed.

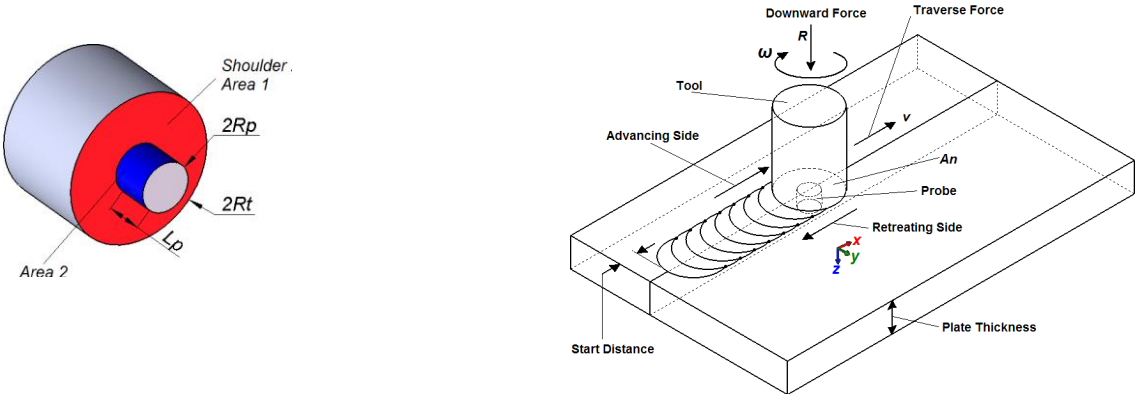

(*a*) (*b*)

Figure 1. FSW process: (*a*) welding tool geometry and (*b*) FSW process parameters.

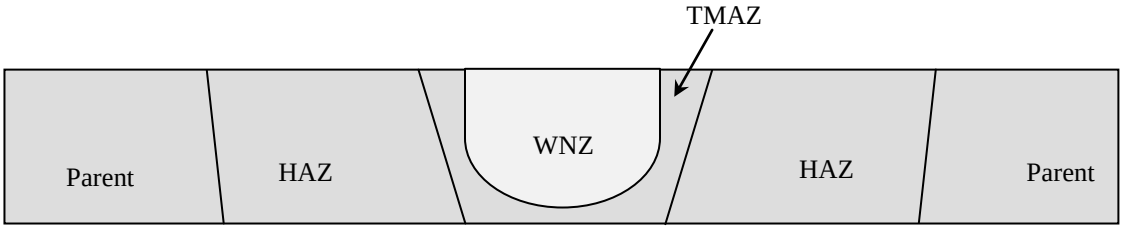

Figure 2. FSW process zones: Heat Affected Zone (HAZ), Thermomechanically Affected Zone (TMAZ) and Weld Nugget Zone (WNZ).

Russell and Shercliff (1999) assess the heat generated by considering a friction force promoted by a constant stress at the interface tool-workpiece which value is equal to the material yield stress at high temperature. Russell (2000) presents a detailed study of the several FSW heat generation mechanisms. Vilaça *et al.* (2005) use an iterative process to adjust a point heat source parameters by minimizing the error obtained from experimental data and model results.

Xu e Deng (2002) presents a tridimensional numerical model based on the finite element method to study the mechanical behavior of the welded material. Non-linearities, like large displacements and temperature dependent, properties are considered. The authors use an uncoupled model as the thermal phenomenon is not considered and temperature data obtained from experimental analysis is used as a prescribed loading.

Zhu e Chao (2003) proposes a heat source model where the heat flux presents a linear distribution through the radial direction. The heat source amplitude is adjusted by comparing results obtained using a thermal finite element model with experimental data obtained from thermocouples. Temperature data is then used as a prescribed loading in a finite element thermoelastoplastic model to obtain the stress field. As well as for the previous model, this is an uncoupled approach.

Buffa *et al.* (2006*a*, 2006*b*) present a coupled model for a rigid-viscoplastic material where the heat generation is dependent on the tool-workpiece friction and the plastic strain promoted by the process. Stress and plastic strain fields are predicted by this coupled model.

In this article, the heat source model proposed by Russel (2000) is modified to incorporate a nonhomogeneous linear distribution for the heat generation contributions associated to tool-workpice friction and workpiece plastic strain. The proposed heat source is used in bidimensional and tridimensional finite element models and applied to study the welding of two aluminum plates. The model is general and can be used to predict the temperature distribution generated by the FSW process in welded plates. Important characteristics of the joint, like TAZ extension, can be predicted for different FSW process parameters, like tool geometry and speed, and for different workpieces geometries and materials.

2. HEAT SOURCE

Accurate prediction of residual stress, distortion, and strength of welded structures require an accurate analysis of the thermal cycle. The importance of an adequate model for the weld heat source in the analysis of the thermal cycle has been emphasized by several investigators (Pavelik *et al.*, 1969; Goldak *et al.*, 1984; Ronda and Oliver, 2000). For traditional welding processes some authors represent the heat source as a geometric distribution of heat flux. Pavelic *et al.* (1969) suggested a Gaussian surface flux distribution disc. Friedman (1975) presents an alternative form for the Pavelic model expressed in a moving coordinate system, with the origin located at the center of the heat source. Goldak

et al. (1984) presents a more accurate model comprising a non-axisymmetric three-dimensional "double ellipsoidal power density distribution" for moving weld heat sources based on a Gaussian distribution of power density in space.

Although there are several works that present experimental data for FSW process, the modeling of the FSW heat source is not well established (Russel, 2000; Mishra and Mahoney, 2007). The majority of the models consider a heat source distributed along the tool surface and that the heat generation occurs at the interface by friction and/or at a thin superficial layer by viscous dissipation. Hypotheses usually adopted are: a symmetric distribution and the effects of the metal flow in the heat generation are not considered.

The boundary conditions at the tool-workpiece are very complex and can be either slipping contact or sticking friction or a combination of both. In the first one the tool rotates at a higher speed than the material workpice whereas in the second both the tool and the local material have the same speed.

There are three major mechanisms that contribute for the heat source: (1) friction at the shoulder-workpiece interface (q_S); (2) friction at the probe-workpiece interface (q_P); and (3) plastic strain at the piece (q_{ϵ_p}). Russell (2000) presents a simple analytical model to represent these mechanisms.

In this work a proposed model based on Russell model (Russell, 2000) is adopted. The model considers some improvements like the dependence of the heat source contributions on the distance from the tool center. Some hypotheses are adopted: the representation of the material behavior through a perfectly plastic material without hardening model and the integrally transformation of mechanical power in thermal power without any loss.

Heat generation contributions associated to the friction between the shoulder-workpiece interface are obtained from a material strip with a width *dr* located at a distance *r* from the tool center, considering translational and rotational relative movements between the tool and the workpiece. For the first one a constant translational relative speed, v_{trans}, is considered while for the second one a linear circumferential relative speed distribution, $v_{rot}(r)$, is considered, as shown in Fig. 3.

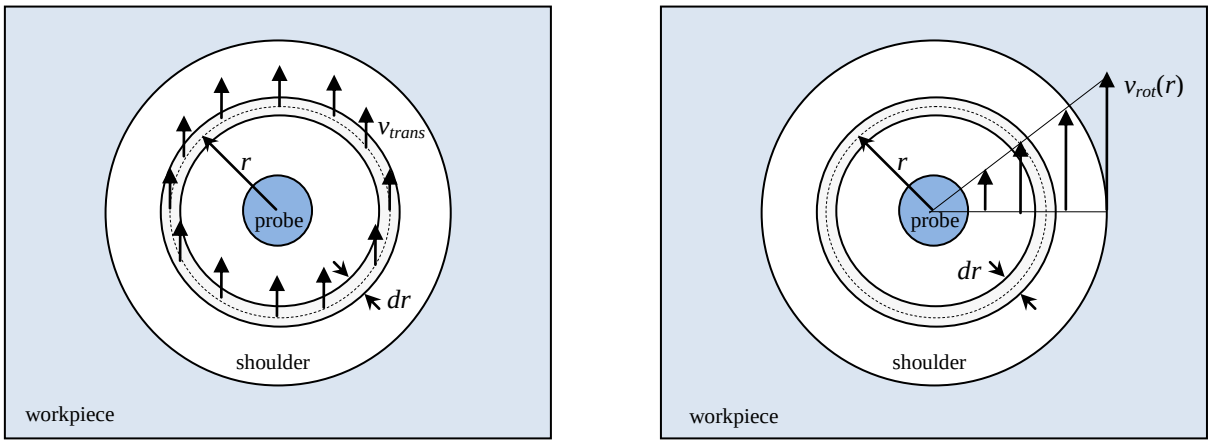

(*a*) (*b*)

Figure 3. Material strip with a width *dr* at distance *r* from the tool center: (*a*) constant translational speed, v_{trans}, and (*b*) linear circumferential speed distribution.

Therefore, considering that a constant circumferential shear stress acting on the workpiece material with a magnitude equal to the shear yield stress at the process temperature (S_Y^{Shear}), the heat power associated to translational and rotational contributions, generated at the annular region of Fig. 3 with a width *dr*, can be represented by:

$$dq_{Shoulder}^{Transl} = S_Y \pi\, r\, dr\, v_{transl} \tag{1}$$

$$dq_{Shoulder}^{Rot} = \pi\, S_Y\, \omega\, r^2\, dr \tag{2}$$

where S_Y is the yielding stress ($S_Y^{Shear} = S_Y/2$, from *Tresca* criterion), v_{transl} the tool translational speed and ω the tool rotational speed.

The proposed model considers that the contributions associated to friction at the probe-workpice interface and to the plastic strain developed in the workpiece are complementary and three conditions can be achieved: (1) a stick condition where there is no slip between the probe and the workpiece; (2) a slip condition, where a slip condition is observed between both surfaces; and (3) an intermediary condition where stick and slip are both present. A stick factor, δ, similar to the one used by Nadan *et al.* (2006) is introduced to permit the inclusion of these three conditions in the model. This factor represents the relative amount of heat generated by plastic strain developed in the workpiece in comparison to the amount of heat generated by the friction at the probe-workpiece interface. Therefore, for these two heat generation contributions, when $\delta = 1$ a limit condition of integral stick is achieved and an integral amount of heat generated by the

plastic strain developed in the workpiece is considered, whereas when $\delta = 0$ a limit condition of integral slip is achieved and an integral amount of heat generated by the friction at the probe-workpice interface is considered. Through this parameter it is possible to establish intermediary conditions between stick and slip conditions. The amount of stick can be assessed through fitted experimental data (Deng *et al.*, 2001).

The contributions associated to the friction at the probe-workpiece interface, heat generation can be represented by:

$$q_p = (1-\delta)\left[\pi\, S_Y\, \omega\, L_p\, (R_p)^2\right] \tag{3}$$

where L_p and R_p are, respectively, the length and the radius of the probe. This equation considers that a constant circumferential shear stress acts on the material in contact with the probe surface, with a magnitude equal to the shear yield stress at the process temperature (S_Y^{Shear}).

For the contribution of the heat generated by the plastic power developed in the workpiece, the model considers that the mechanical power is integrally transformed in thermal power. The intensive plastic strain occurs inside a material region named *weld nugget*. Figure 4 presents a schematic representation and a macrograph of the *weld nugget*. The use of these simple models requires the calibration of the model, and several parameters, like the weld nugget dimension, must be estimated from experimental data.

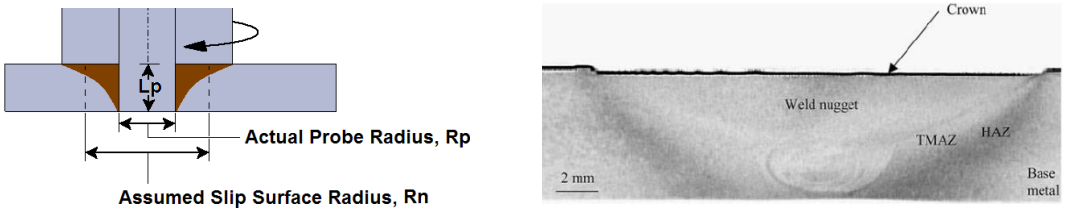

(*a*) (*b*)

Figure 4. Weld nugget parameters (*a*) and *weld nugget* macrograph (Chen and Kovacevic, 2003) (*b*).

The stress/strain state present in the workpiece is very complex and some hypotheses are adopted: (*i*) the process promote a circumferential linear displacement distribution (u) in the annular region between the probe interface ($r = R_p$) and the *weld nugget* limit ($r = R_n$), as shown in Fig. 5*a*; and (*ii*) the annular region is submitted to a constant circumferential stress state with a magnitude equal to the material yield stress limit (S_Y), as shown in Fig. 5*b*, which presents a straightened representation of a *dr* width material strip.

The circumferential linear displacement distribution, $u(r)$, and the strain rate, $\dot{\varepsilon}\,(r)$, in the annular region between the probe interface ($r = R_p$) and the *weld nugget* limit ($r = R_n$), can be written as:

$$u(r) = \left(\frac{R_n - r}{R_n - R_p}\right) u_p \quad ; \qquad \dot{\varepsilon}\,(r) = \frac{\dot{u}\,(r)}{L_0} = \frac{v\,(r)}{2\pi r} = \left(\frac{R_n - r}{R_n - R_p}\right)\frac{v_p}{2\pi r} \qquad \text{for } R_p \le r \le R_n \tag{4}$$

where u_p and v_p are, respectively, the circumferential displacement and speed at the probe-workpiece interface.

Considering that large strains are present in the *weld nugget* annular region, elastic strains can be disregarded. Therefore, $\varepsilon = \varepsilon^p + \varepsilon^e \cong \varepsilon^p$, where ε^p is the plastic strain part and ε^e is the elastic strain part. The proposed model considers a maximum value of plastic strain at the material in contact with the probe and a null value outside the *weld nugget* region, as show in Fig. 5*c*. The plastic power generated by plastic strain developed at the workpiece is equal to $\sigma\dot{\varepsilon}_p(r)$, and the associated heat generated can be written as:

$$q_{\epsilon_p}(r) = \delta\left[\sigma\dot{\varepsilon}_p(r)\right] = \delta\,\frac{S_y\, R_p\, \omega}{2\pi r}\left[\frac{R_n - r}{R_n - R_p}\right] \qquad \text{for } R_p \le r \le R_n \tag{5}$$

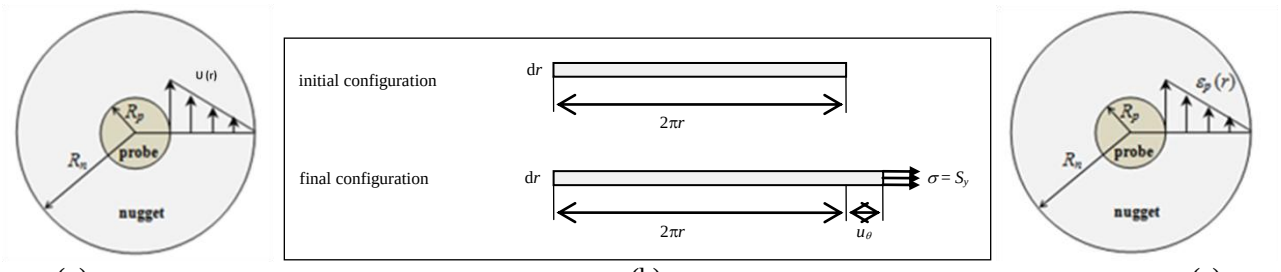

(*a*) (b) (*c*)

Figure 5. *Weld nugget* region: (*a*) linear displacement distribution, (*b*) strain in a strip material with *dr* width and (*c*) linear plastic strain distribution.

3. NUMERICAL MODEL

Two numerical models based on the finite element method are presented to study the temperature distribution in plates welded by the FSW process: an axisymmetric bidimensional and an tridimensional model. The proposed models are applied to the welding of two aluminum AA2014-T6 6.35 thickness plates by FSW process, reproducing the process studied by Russel (2000) where 5 thermocouples are incorporated to the plates to measure temperature evolution during the process. The geometry, the thermocouples position, the material properties and process parameters are presented in Fig. 6 and Tables 1 and 2, respectively.

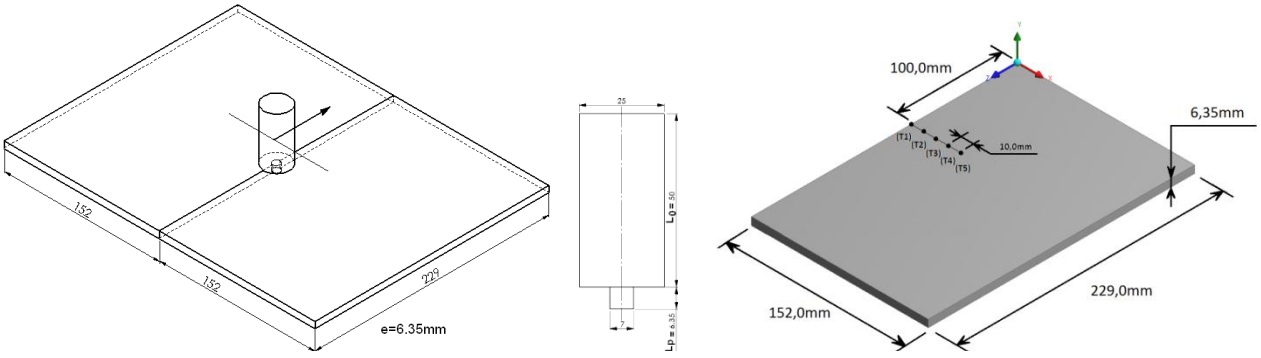

(*a*) (*b*)

Figure 6. (*a*) Welded plates and tool geometry. (*b*) thermocouple positions (Russell ,2000).

Table 1. AA2014-T6 material properties (Russell, 2000).

Material Properties	AA2014 -T6	HS Steel Tool
Thermal conductivity, K (W/mK)	155	20
Yield stress at room temperature, $S_Y^{RoomTemp}$ (MPa)	400	-
Yield stress at FSW temperature, $S_Y^{FSW\ Temp}$ (MPa)	12	-
Onset melting temperature, T_m (ºC)	507	-

Table 2. FSW parameters – AA2014-T6 (Russell, 2000).

FSW Parameters	Value
Tool radius, R_t (mm)	12.5
Welding speed, v (mm/s)	1.33
Rotational speed, ω (rpm)	500
Total power generated, q_{gen} (W) ≈	1300
Heat flux fraction of the working tool, f	0.85
Effective power of the working tool, q_{net} (W)	1105

The axisymmetric bidimensional model is chosen as a first approach. The hypothesis of axisymmetry can be justified by the fact that the tool rotational motion introduces a small perturbation on the temperature radial distribution. The model considers a thermal steady-state response and do not contemplate the effects of translational motion. Numerical simulations are performed with commercial finite element code ANSYS (Ansys, 2010), employing thermal element PLANE55 (4 nodes with a single degree of freedom – temperature - per node) for spatial discretization. Figure 7 presents the geometry of the model composed by 5 areas. Area A1 represents the tool and areas A2 to A5 the plate. Areas A3 to A5 are used to control the mesh discretization. Figure 8 presents the mesh used after a convergence analysis. Convection boundary conditions are applied to the surface. The present analysis considers the 3 heat source mechanisms described in section 2 associated to equations (2), (3) and (5). As the effects of translational motion are not contemplated, equation (1) is not considered.

Heat generation contributions are applied to selected elements as a heat generation rate through ANSYS command BFE (element body force load, using the label HGEN for heat generation rate body load type). Contribution $q_{Shoulder}^{Rot}$ is applied to the elements in areas A4 and A5 whereas contribution q_{ϵ_p} is applied to elements in area A3 of Fig. 7*a*. For q_p contribution is applied to elements adjacent to lines L2 and L3 of Fig. 7*b*. A convection coefficient, h, of 30 W/m^2 ºC is adopted for the aluminum plate free surfaces. At the aluminum plate bottom an equivalent convection coefficient, h, of

250 W/m^2 ºC is adopted to represent the heat transfer between the plate and the base (*backing plate*). Finally, for the top of the tool an equivalent convection coefficient, *h*, of 1500 W/m^2 ºC is adopted to represent the heat transfer between the tool and the mandrel (Khandkar *et al.*, 2003; Hamilton *et al.*, 2008).

(*a*) (*b*)

Figure 7. Model geometry (*a*) and detail (*b*). Bidimensional model.

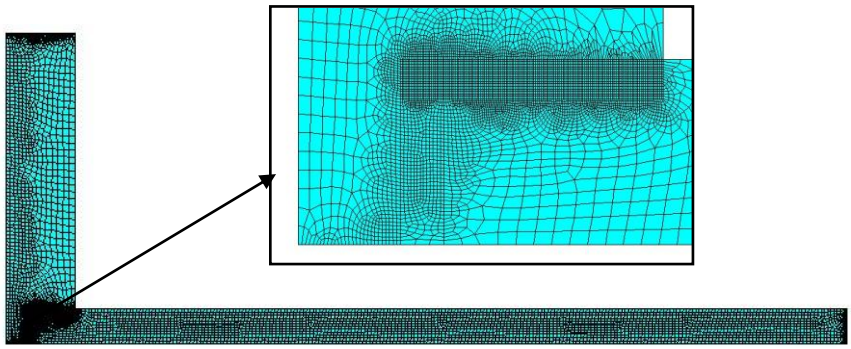

Figure 8. Finite element mesh. Bidimensional model.

The tridimensional model considers a symmetry condition at the welding path. The model considers thermal transient response and contemplate the effects of translational motion. Numerical simulations are performed with commercial finite element code ANSYS (Ansys, 2010), employing thermal element SOLID70 (8 nodes with a single degree of freedom – temperature - per node) for spatial discretization. Figure 9*a* presents the mesh used after a convergence analysis whereas Fig. 9*b* presents the convective boundary conditions.

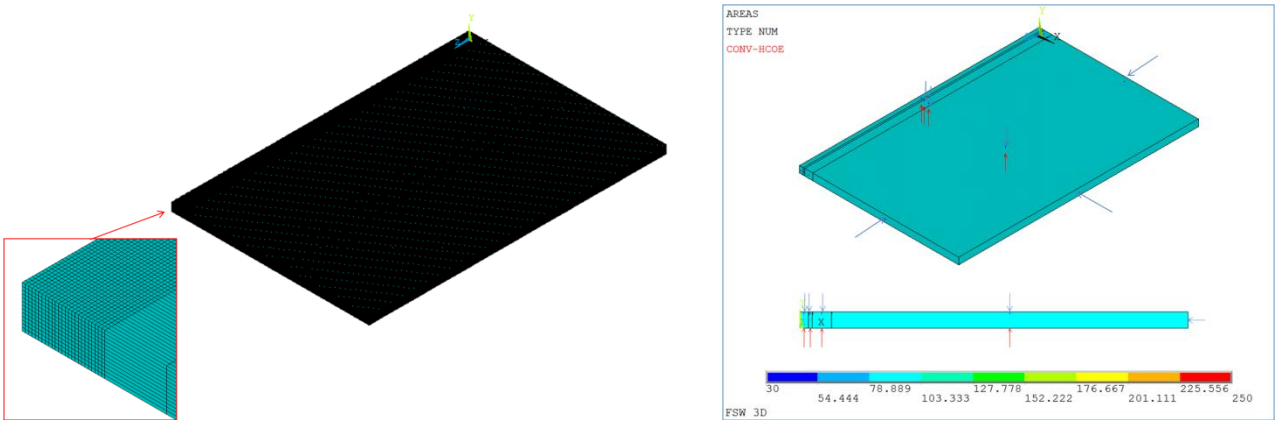

(*a*) (*b*)

Figure 9. Finite element mesh (*a*) and convective boundary conditions (*b*). Tridimensional model.

Heat generation contributions are applied to selected elements as a heat generation rate through ANSYS command BFE (element body force load, using the label HGEN for heat generation rate body load type). The present analysis considers the 4 heat source mechanisms described in section 2 associated to equations (1-3) and (5). A numerical

routine developed in APDL programming language (Ansys, 2010) is used to apply the 4 heat generation contributions ($q_{Shoulder}^{Transl}$, $q_{Shoulder}^{Rot}$, q_{ϵ_p}, q_p) as the source moves through the plate.

The material is assumed to be at an initial temperature of 20ºC, which is similar to the ambient temperature, and convective boundary conditions are applied to lines associated to the plate surface and tool surface. Both models consider the yield stress at FSW temperature ($S_Y^{FSW\ Temp}$).

4. NUMERICAL SIMULATIONS

Figure 10*a* presents a comparison between experimental data obtain by Russell (2000) and numerical results obtained by bidimensional (2D) and tridimendional (3D) models. Coordinate *x* measures the perpendicular distance from the welding path. Experimental data is collected at the time instant, *t* = 76 s, when the tool walk through the thermocouples line (at a distance of 100 mm from the plate end - Fig. 6*b*). The numerical data presented for 2D model is the temperature distribution for the steady-state solution whereas for 3D model is the temperature distribution at the thermocouples position. Figure 10*b* shows temperature distribution for 3D model while Figs. 10*c* and 10*d* present temperature distribution for 2D and 3D models at the same correspondent cross section (time instant *t* = 76 s for 3D model). A good agreement can be observed between numerical and experimental data.

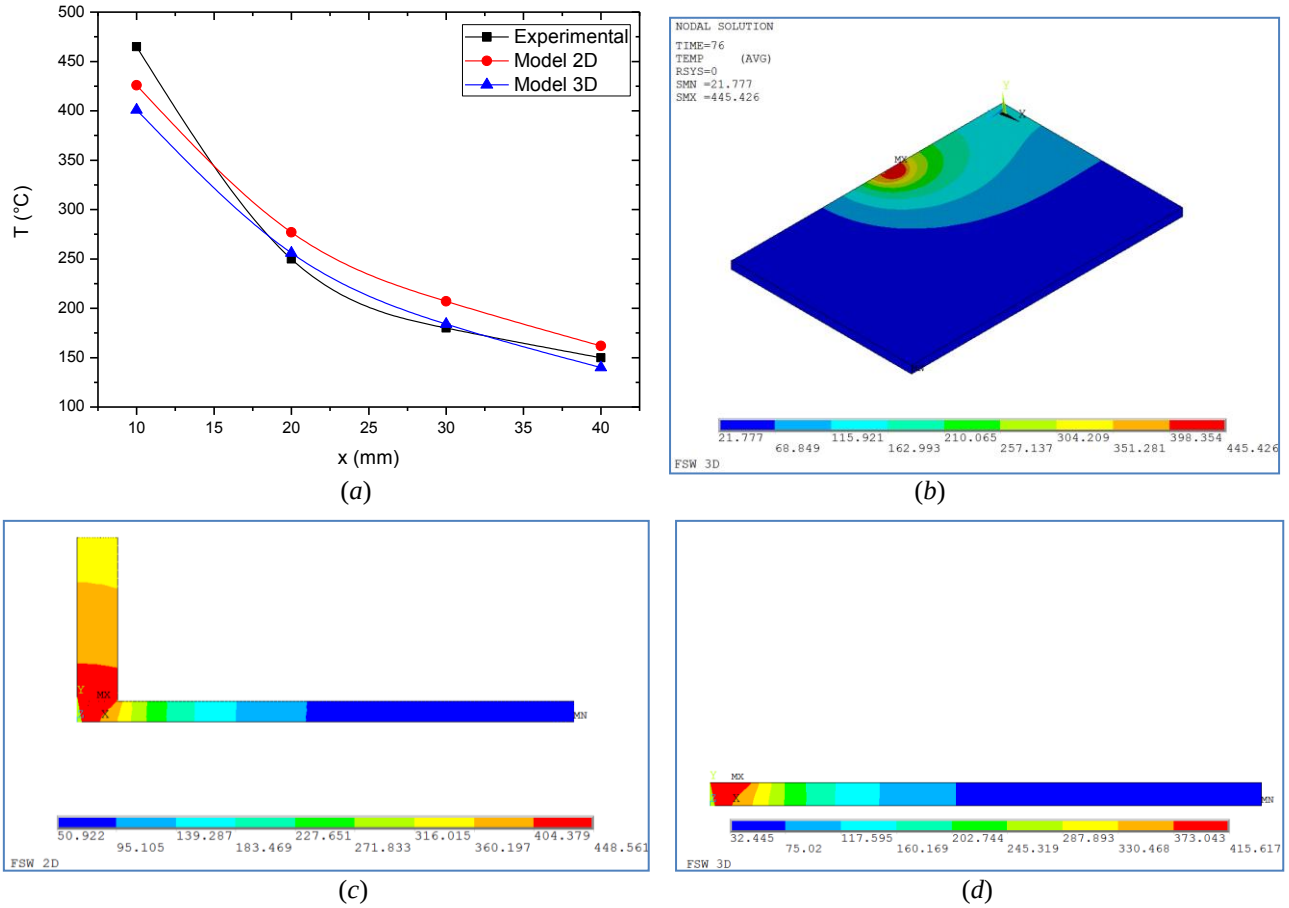

(*a*) (*b*) (*c*) (*d*)

Figure 10. (a) Temperature values at the thermocouples position for experimental and numerical data. Temperature distributions for: (*b*) 3D model, (c) 2D model and (d) 3D model at a cross section (*t* = 76 s for 3D model).

Figure 11 shows the temperature evolution at thermocouples positions for experimental data and numerical results obtained from 3D model. TP*i* and P*i* represents, respectively, thermocouple data and numerical data at point *i* (*i* = 1,., 5 – Fig. 6*b*). A good agreement can be observed. The interruption of thermocouple TP1 data is associated to its destruction during the passage of the tool.

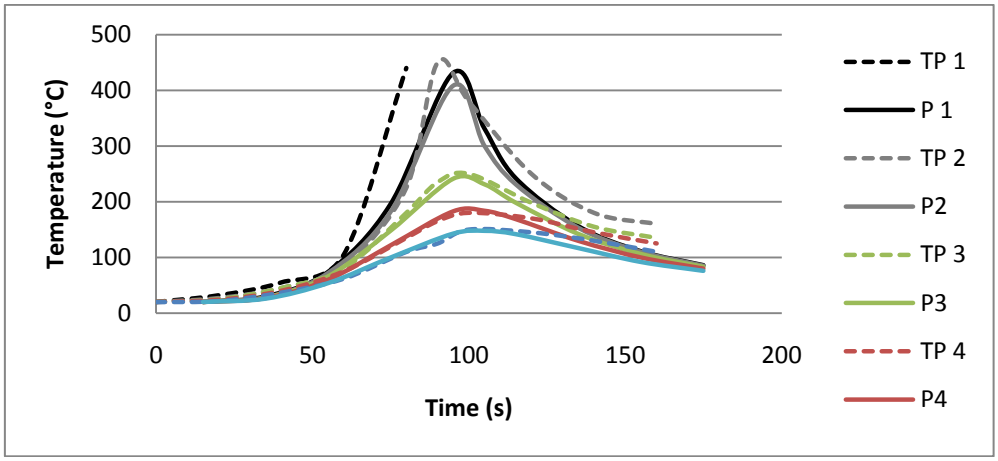

Figure 11. Temperature evolution at thermocouples positions for experimental and numerical results obtained from 3D model.

At this point the proposed models are used to study the parameters influence on the temperature distribution promoted by the FSW process.

Figures 12*a-c* shows, respectively, the effect of rotational speed, translational speed and stick factor on the temperature distribution using the 3D model. Comparing the rotational and translational speed effects, results shows that the first one presents a larger influence on temperature. As expected, higher temperature values are obtained for higher rotational speeds and for lower translational speeds. For the stick factor, higher temperature values are observed when $\delta = 0$, which is associated to a total slip condition where the q_p contribution is integral.

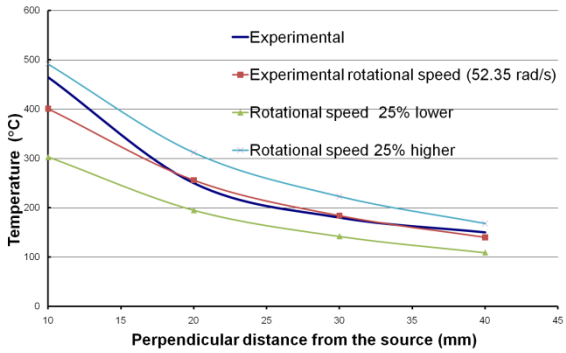

(*a*)

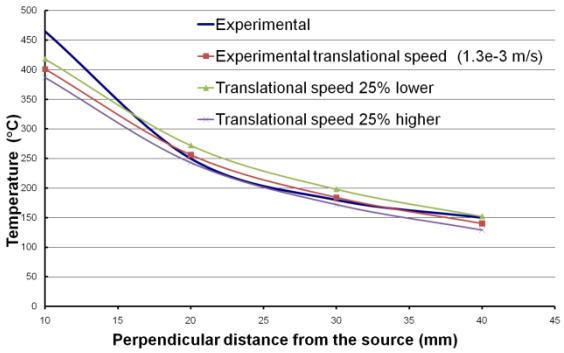

(*b*)

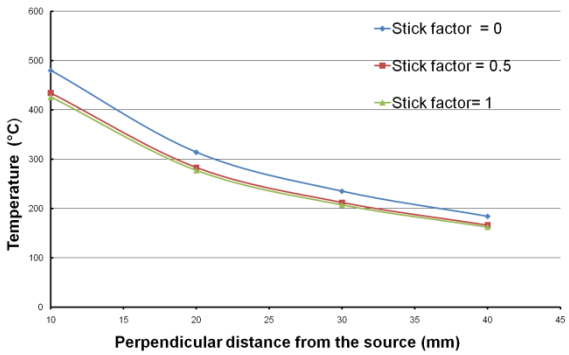

(*c*)

Figure 12. Effect of rotational speed (*a*), translational speed (*b*) and stick factor (*c*) on the temperature distribution. 3D model.

Figure 13 shows the cross section temperature distribution for the 3 rotational speeds presented in the results of Fig. 12: 500 rpm, 25% lower and 25% higher. Red and green regions are associated to the HAZ, defined as the region where temperature is higher than half the melting temperature: T > 253.3 ºC (Espósito, 2006).

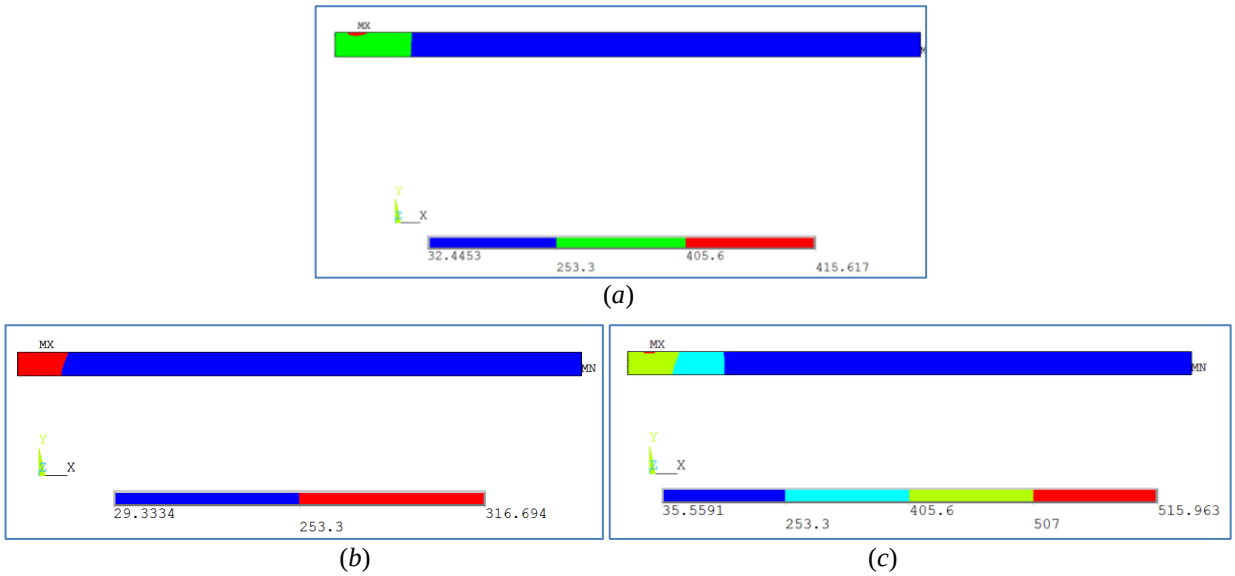

(*a*)

(*b*) (*c*)

Figure 13. Effect of the rotational speed on HAZ: (*a*) nominal rotational speed (500 rpm), (*b*) 25% lower and (*c*) 25% higher. 3D model

Figures 14*a* and 14*b* shows, respectively, the effect of plate thickness and nugget radius on the temperature rise associated to heat generation contribution promoted by the plastic strain (q_{ϵ_p}). Results show that for the problem analyzed, the amount of heat generated by the plastic strain is small when compared with the one generated by friction at the probe and the shoulder. As expected, higher values of temperature are obtained for larger thickness plates and larger *nugget radius* as the material volume submitted to plastic strain is larger.

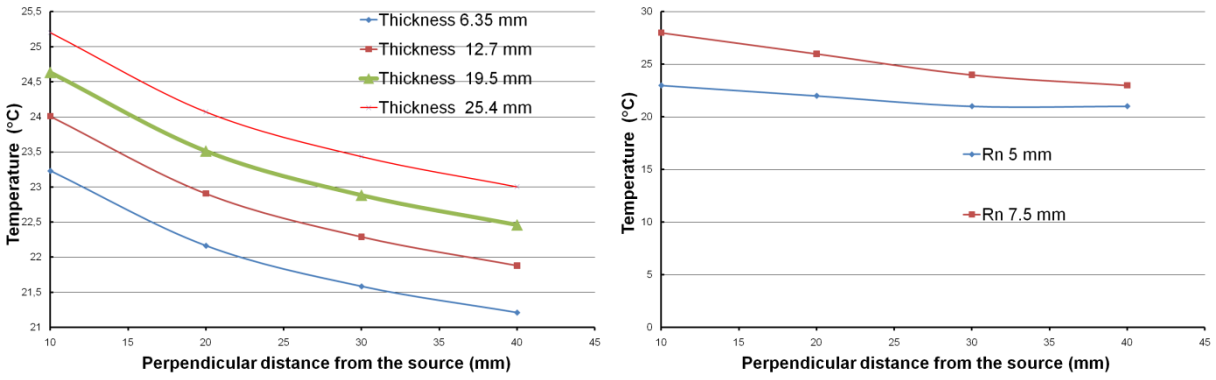

(*a*) (*b*)

Figure 14. Effect of plate thickness (*a*) and *nugget radius* (*b*) on the temperature rise associated to plastic strain. 2D model

5. CONCLUSION

Two finite element models are proposed to study the temperature distribution in FSW welded plates. The models consider the contribution of the several phenomena present in the process, as the heat generated by the tool-workpiece friction and the workpice plastic strain. The proposed model for the heat source presents a linear distribution and is applied to study the temperature distribution for the welding of aluminum plates. For the studied conditions, rotational

speed is the FSW process parameter that presents larger effects on the workpiece temperature evolution. Numerical results show that the model is in close agreement with experimental results, indicating that the model is capable of capturing the main characteristics of the process. The proposed model can be used to predict important process characteristics, like the TAZ (Thermal Affected Zone), as a function of the welding parameters.

6. ACKNOWLEDGEMENTS

The authors would like to acknowledge the support of the Brazilian Research Agency CNPq and ESSS.

7. REFERENCES

ANSYS Inc., *Analysis Guide*, Release 12, 2010.

Buffa G., Hua J., Shivpuri R., Fratini L., 2006*a*, "Design of the stir welding tool using the continuum based FEM Model", *Materials Science and Engineering*, 10.

Buffa G., Hua J., Shivpuri R., Fratini L., 2006*b*, "A continuum based model for friction stir welding – model development", *Materials Science and Engineering*, 10.

Chen, C.M.; Kovacevic, R., 2003; "Finite element Modeling of Friction Stir Welding – termal and thermomechanical Analysis", *International Journal of Machine Tools & Manufacture*, pp.1319-1326.

Colegrove, P; Painter, M; Graham, D.; Miller, T., 2000; "Three-dimensional flow and thermal modelling of the friction stir welding process", *Proceedings of the Second International Symposium on Friction Stir Welding*, Gothenburg, Sweden.

Deng, X. e Xu, S., 2001; "Solid Mechanics Simulation of Friction Stir Welding Process", *Trans. NAMRI/SME SME*, 29, 631–638.

Deng, Z., Lovell, M.R. E Tagavi, K.A., 2001; "Influence of Materials Properties and Forming Velocity on the Interfacial Slip Characteristics of Cross Wedge Rolling", *Manuf. Sci. Eng.*, v.123, pp. 647-653.

Espósito, I. M., 2006; "Caracterização e Cinética de Recristalização da Liga de Alumínio 6063 Após Tratamentos Térmicos", IPEN, Dissertação de Mestrado.

Friedman, E., 1975; *Jounal of Pressure Vessel Technology*, Trans ASME, Vol. 97, pp.206-213.

Goldak, J., Chakravarti, A. and Bibby, M., 1984, "A New Finite Element Model for Welding Heat Sources", *Metallurgical Transactions B*, Volume 15B, June 1984, pp. 299–305.

Hamilton, C., Dymek, S. and Sommers, A., 2008; "A thermal model of friction stir welding in aluminum alloys", *International Journal of Machine Tools & Manufacture*, 48, 1120–1130.

Khandkar, M.Z.H., Khan, J.A. and Reynolds, A.P., 2003; "Prediction of temperature distribution and thermal history during friction stir welding: input torque based model", *Science and Technology of Welding and Joining*, Vol. 8, No. 3, pp.165-174.

Mishra, R.S. and Mahoney, M.W., 2007, *"Friction Stir Welding and Processing"*, ASM.

Nandan, R.; Roy, G.G.; Debroy, T., 2006; "Numerical Simulation of Three-Dimensional Heat Transfer and Plastic Flow During Friction Stir Welding", *Metallurgical and Materials Transactions A*, v.37A, pp.1247-1259.

Nandan, R., Debroy, T., Bhadeshia, H.K.D.H, 2008; "Recent Advances in Friction Stir Welding – Process, Weldment Structure and Properties", *Progress in Materials Science*, pp.980-1023.

Pavelic, Z., Tanbakuchi, R., Uyehara, O.A. and Meyers, P.S., 1969**,** *Welding Journal Research Supplement*, Vol. 48, pp. 295s–305s.

Ronda, J. and Oliver, G.J., 2000, "Consistent Thermo-Mechano-Metallurgical Model of Welded Steel with Unified Approach to Derivation of Phase Evolution Laws and Transformation-Induced Plasticity", *Comput. Methods Appl. Mech. Engrg.* Vol. 189, pp. 361-417.

Rosenthal, D., 1946, "The theory of moving sources of heat and its. applications to metal treatments", *Transactions of the ASME*, p.849- 866.

Russelll, J. M., 2000; "*Development and Modelling of Friction Stir Welding"*, Thesis, University of Cambridge.

Russelll, M.J.; Sheercliff, H.R., 1999; "Analytic modeling of microstructure development in friction stir welding", *Proceedings of the First International Symposium on Friction Stir Welding*, Thousand Oaks, CA, USA.

Vilaça, P., Quintino, L. e dos Santos, J.F., 2005; "iSTIR—Analytical Thermal Model for Friction Stir Welding", *Journal of Materials Processing Technology*, 169, 452–465.

Xu, S. e Deng, X. 2002; "A three-dimensional model for the friction-stir welding process", *Proceeding of the 21st Southeastern Conference on Theoretical and Applied Mechanics (SECTAM XXI)*, pp. 699–704.

Zhu, X. K.; Chao, Y.J., 2003; "Numerical simulation of transient temperature and residual stresses in friction stir welding of 304L stainless steel", *Journal of Materials Processing Technology*,V. 146, 2,pp. 263-272

8. RESPONSIBILITY NOTICE

The authors are the only responsible for the printed material included in this paper.